Engineering Graphene Wrinkles for Large Enhancement of Interlaminar Friction Enabled Damping Capability

Engineering Graphene Wrinkles for Large Enhancement of Interlaminar Friction Enabled Damping Capability

Wenjiang Lu,[†] Faxiang Qin,[†,*] Yunfei Wang,[†] Yang Luo,[†] Huan Wang,[†] Fabrizio Scarpa,[‡] Jixue Li,[§] Raffaella Sesana,[T] Francesca Cura,[T] and Hua-Xin Peng[†,*]

[†]Institute for Composites Science Innovation (InCSI), School of Materials Science and Engineering, Zhejiang University, 38 Zheda Road, Hangzhou, 310027, PR. China, [‡]Bristol Composites Institute (ACCIS), University of Bristol, BS8 1TR Bristol, UK, [§]Center of Electron Microscopy and State Key Laboratory of Silicon Materials, School of Materials Science and Engineering, Zhejiang University, 38 Zheda Road, Hangzhou 310027, PR, China, [T]Politecnico di Torino, corso duca degli Abruzzi 24, 10129 Torino, Italy

Address correspondence to faxiangqin@zju.edu.cn (FXQ)
hxpengwork@zju.edu.cn (HXP)

ABSTRACT: Graphene nanoplates are hoped-for solid lubricants to reduce friction and energy dissipation in micro- and nano-scale devices benefiting from their interface slips to reach an expected superlubricity. On the contrary, we propose here by introducing engineered wrinkles of graphene nanoplates to exploit and optimize the interfacial energy dissipation mechanisms between the nanoplates in graphene-based composites for enhanced vibration damping performance. Polyurethane (PU) beams with designed sandwich structures have been successfully fabricated to activate the interlaminar slips of wrinkled graphene-graphene, which significantly contribute to the dissipation of vibration energy. These engineered composite materials with extremely low graphene content (~0.08wt%) yield a significant increase of quasi-static and dynamic damping compared to the baseline PU beams (by 71% and 94%, respectively). Friction force images of wrinkled graphene

oxide (GO) nanoplates detected *via* Atomic Force Microscope (AFM) indicate that wrinkles with large coefficients of friction (COFs) indeed play a dominant role in delaying slip occurrences. Reduction of GO further enhances the COFs of the interacting wrinkles by 7.8% owing to the increased effective contact area and adhesive force. This work provides a new insight on how to design graphene-based composites with optimized damping properties from the microstructure perspective.

KEYWORDS: wrinkled graphene, interfacial friction, coefficient of friction, sandwich structure, damping properties

INTRODUCTION

Graphene is widely used as a solid lubricant in micro- and nano-scale mechanical devices, and decreasing the friction of graphene modified surfaces to reach superlubricity is currently a constant effort to improve the lubricating performance of MEMS (micro-electromechanical) and NEMS (nano-electromechanical) systems.[1-5] This involves frictional slips between graphene nanoplates and two major factors are proposed to influence their interfacial friction behavior. The first is the presences of interlaminar interactions (Van der Waals force,[6] electrostatic attraction,[7] and interlayer radial loading[8]) and the second pertains to the conditions of the surface (defects,[9, 10] roughness,[11] edge steps,[12] and pucker morphology[13-15]). The weak interlaminar interactions and less complex surface conditions have been demonstrated to decrease the friction in graphene systems. For examples, Wang *et al.* have proposed to decrease interlayer interactions by using hydrogen-passivated graphene, featured with a decreased friction.[16, 17] Similar results have also been reported by using fluorine-passivation in Sen's work.[18] Zeng *et al.* have suppressed graphene puckering by strengthening interactions with the substrate to decrease friction.[19]

There is a keen interest to develop technologies for reducing the friction of graphene surfaces. By contrast, the activities described in this work focus on increasing the friction to optimize the interfacial energy dissipation mechanisms between graphene nanoplates in graphene-based nanocomposites for enhanced damping performance. Graphene nanomaterials serve the purpose very well for the following reasons. (i) The extreme large surface area and high strength make graphene a suitable filler for polymers to provide enhanced damping performance.[20, 21] (ii) The low mass density avoids weight penalty, which is crucial in particular for aerospace applications. The graphene-graphene interfacial friction is an important energy dissipation mechanism,[22, 23] yet it is scarcely reported and the most work relating to this behavior found in the open literatures focus on the simulations between ideal flat graphene sheets.[2, 24, 25] We describe here how to enhance the interlayer friction behavior of graphene nanoplates by introducing wrinkles through oxidization and therefore provide high frictional energy dissipation, as the puckering of graphene is capable of increasing friction.[1, 14, 15] By further adjusting the interlaminar interaction *via* the reduction process, we can obtain remarkable enhancement in damping performance of graphene nanocomposites since the relative slips between wrinkled graphene nanoplates are engineered. The potential of wrinkling graphene as a method to tailor multifunctional properties, such as super-hydrophobicity, capacitive, sensing, adsorbing, has been explored in several studies.[26-29] Despite of some studies on engineering wrinkle for controlling friction of graphene,[15, 30, 31] to the best of our knowledge, no work has so far focused on the effect of wrinkles in graphene on the damping properties of their composites and elucidated the damping mechanisms from the nanofriction perspective with the aid of atomic force microscope (AFM).

As a demonstrator of a material substrate that would increase its energy dissipation and damping performance by using engineered wrinkled graphene, beams structures made of polyurethane (PU)

have been used here due to its intrinsic high viscoelastic properties.[32] Increased damping properties can be obtained when the beams are in a sandwich form.[33-35] A dip-coating method is adopted to fabricate the sandwich beams, in which graphene or graphene oxide (GO) coatings are represented as the damping core layers. Within the configuration of these designed beams, their quasi-static energy dissipations and damping loss factors exhibit remarkable 71% and 94% increases compared to pristine PU beams, respectively.

RESULTS AND DISCUSSION

Design of The Wrinkled Graphene and Their Sandwich Nanobeams. The formation of wrinkled graphene can be achieved through various methods.[26] Figure 1a depicts how engineered wrinkled graphene has been produced in this work through a facile oxidization and reduction process. The oxidization of graphene nanoplates (GnPs) can produce wrinkles in the nanoplates and the further reduction can adjust the properties of the wrinkles, *i.e.* the shrinking of the wrinkles. By sandwiching damping layers (wrinkled GO coating layers, for example) between two constrained layers of PU matrix (Figure 1b), we can create an efficient molecular damping mechanism that dissipates mechanical energy into heat through the nano-scale deformation of the graphene sheets with relative displacements. The fabrication of the sandwich nanobeams is based on the use of PU beam substrates combined with a dip-coating method (Figure 1c). The critical process is represented by the coating of the damping core layers (especially the one for GO coating). Evaluating the quality of the coating entails three critical factors. (i) The coating morphology: the GO nanoplates should be unfolded, overlapped and evenly attached to the surface of the PU in order to maximize the benefits of their large specific surface area for the GO interface friction. (ii) The number of wrinkles: large numbers of wrinkles are present in GO nanoplates and they could contribute to the

energy dissipation through interface friction. (iii) The bonding strength of the GO-PU interface: this should be sufficient to transform load from the PU matrix and activate the GO-GO slip mechanism when the sandwich nanobeams are subjected to mechanical cyclic deformation.

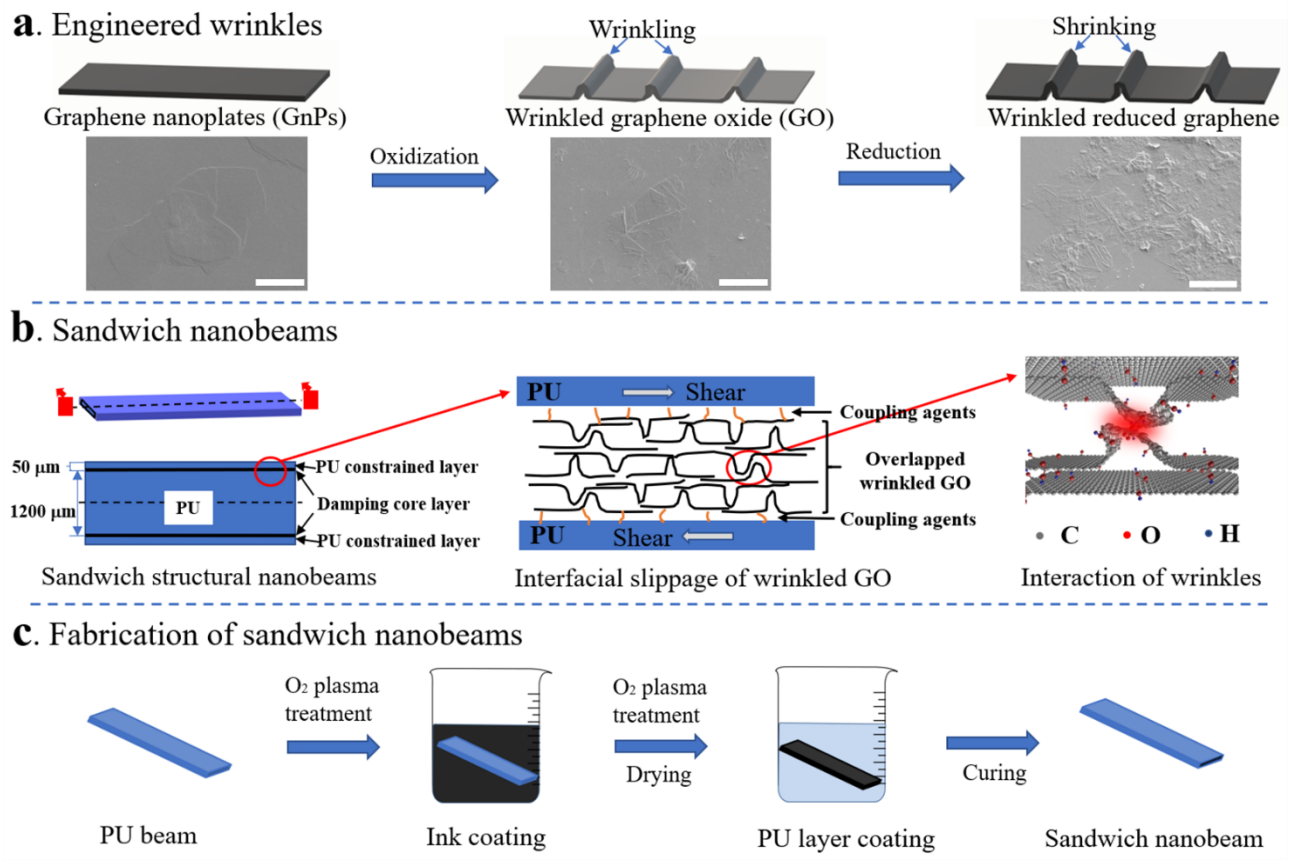

Figure 1. a) Schematics of the engineered wrinkled graphene (oxide) and their corresponding SEM images, scale bar: 5 μm. The oxidization process can wrinkle the GnPs and the wrinkles shrink due to the further reduction progress. b) Illustration of the interfacial slippage energy dissipation of wrinkled GO sandwiched by PU layers. The strong chemical bonds formed by the coupling agents transform the shear load from the PU matrix to the overlapped GO core layer, the interfacial slip between wrinkled GO nanoplates is activated and causes the interactions of wrinkles. c) Flow chart of the fabrication of the sandwich PU nanobeams. The O_2 plasma treatment applied here is to create oxygen contained groups on the pre-coating surface and assist in forming chemical bonds with coupling agents in the PU/GO interfaces.

The as-produced GnPs possess a smooth surface with 5~10 μm in size and ~3.5 nm in thickness

(Figure 2a). After being oxidized, the GO nanoplates assume a rough surface with wrinkles, and their thicknesses increases to ~6.3 nm due to the introduction of oxygen-contained groups on the nanoplates (Figure 2b). The GO nanoplates contain approximately six single sheets of GO, since each one is close to 1nm in thickness.[36] Samples coated with GnPs and GO nanoplates were prepared (Figure 2c-e). Both the flat GnPs and the wrinkled GO nanoplates are uniformly coated on whole smooth pristine PU surface in an unfolded and overlapped manner by using our fabrication processes. Ultrasonication has confirmed the presence of strong GnPs and GO attachments due to the chemical bonds between the PU and the GnPs (GO) created by the coupling agent (Figure S1 in the Supporting Information). All these demonstrate that the pre-conceived damping coatings are successfully obtained by using our ink dip-coating processes. The reasons are multiple and the key one is the preparation of a proper ink coating solution. The dispersion and solubility of the GO are dependent on the polarity and surface tension of the solvent, and the uniform dispersions can be obtained in water.[37-39] Ethylene glycol (EG) was selected as the solvent because of its close polarity and surface tension to water (Table S1 in the Supporting Information). The as-prepared GO nanoplates dispersed in EG with the assistance of 2.5 h ultrasonication are ~ 6 nm in thickness, which are stiff enough to guarantee the nanoplates in an unfolded status and meanwhile maintaining plenty of wrinkles and crumples. A silicane coupling agent was also added to further improve the stability of the ink[37, 40] (Figure S2 in the Supporting Information) and to obtain a strong GO attachment by building chemical bonds between the GO and the PU (combined with O_2 plasma treatment).[41] In addition, the wrinkled morphology of the flexible GO nanoplates also contributes to the good quality of the coating because of the desired undulations[42, 43] (wrinkles, crumples) that can simultaneously impede the self-curling and the reaggregation of the GO.[44-46]

After the GO coating, the beams were dip-coated with the PU acting as a top constraining layer.

SEM images (Figure 2f, g) show that the PU fully wraps the GO-coated beams and produces a uniform layer of thickness ~50 μm. The interfaces of the sandwich beams present high-quality, as the PU layers contact directly with the GO core layer. The GO coating layer is ~100 nm in thickness, which consists of multiple overlapped GO nanoplates. In addition, the PU attached to the GO nanoplates also contributes to the overall thickness of the GO core layers, as their morphology differs from that of pure GO coating membranes (Figure S3 in the Supporting Information). The separated PU phases show that the GO nanoplates are still attached to both sides of the PU surfaces (Figure 2h and Figure S4 in the Supporting Information). This is due to the strong chemical bonds between the PU-GO interfaces created by the coupling agents,[47-49] which are stronger than the interlaminar Van der Waals force between GO nanoplates.[50] The overlapped GO nanoplates in the core layers are therefore exfoliated and delaminated as the PU layers are separated from each other.

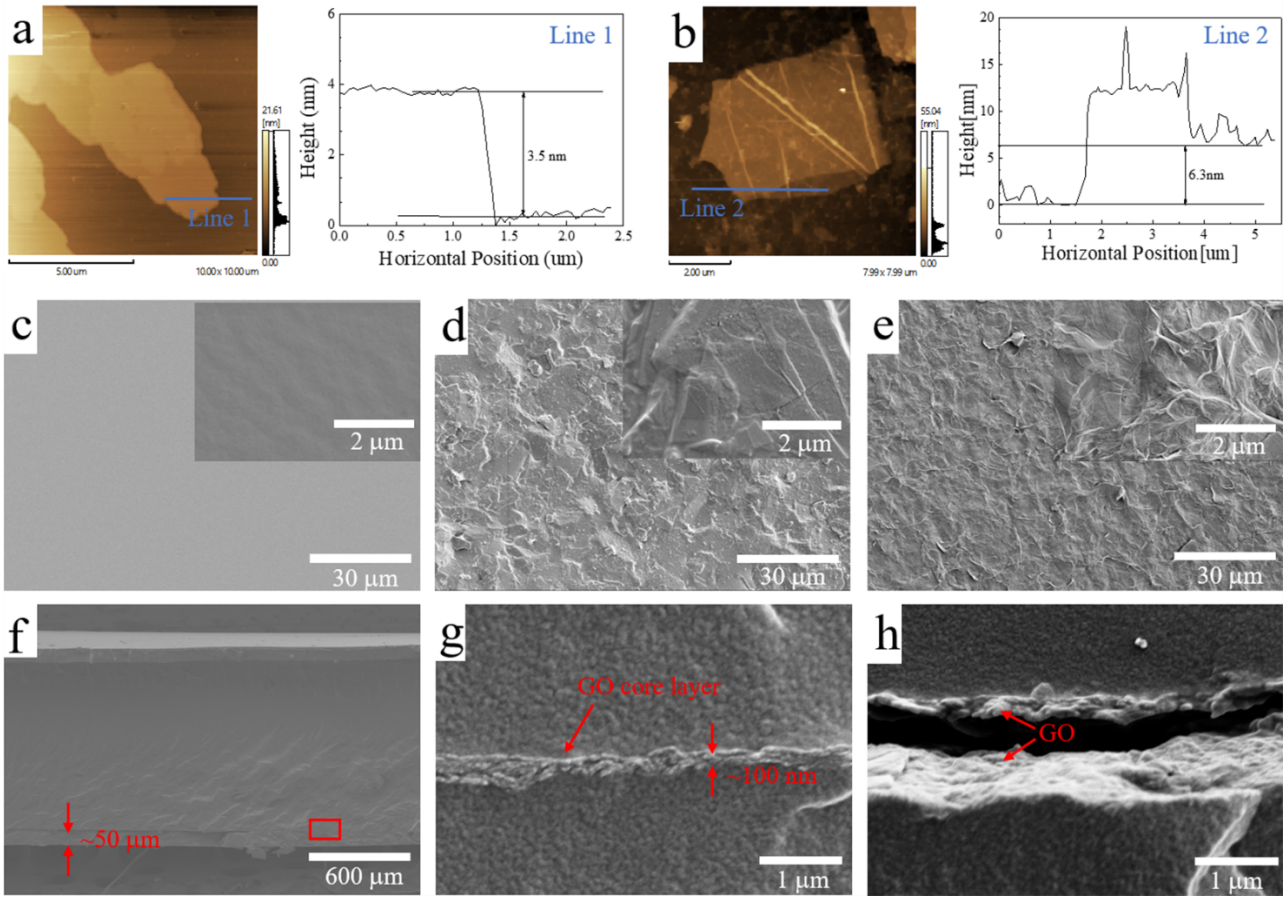

Figure 2. AFM images of as-prepared a) flat GnPs and b) wrinkled GO nanoplates and their corresponding height

profile patterns derived from line 1 and line 2, respectively. SEM images of c) pristine PU surface and morphologies after coating with d) GnPs and e) GO nanoplates. The flat GnPs and wrinkled GO nanoplates are firmly coated on the smooth PU surface in an unfolded and overlapped manner. f-h) Cross-sections of the sandwich nanobeam samples with GO as the core layer and the delaminated GO nanoplates as the PU layers separate from each other.

Most of previously reported simulations of the nanofriction effects in graphene fail to consider large-scale wrinkles occurring on the surface and reveal that the graphene interlaminar shear force is dependent on the interlayer distance, which is related to the number of oxygen-contained functional groups on the graphene sheets.[24] The GO nanoplates after oxidizing the GnPs in this work are however wrinkled, and we have performed an additional reduction process to tailor the properties of the wrinkles by using hydroiodic acid (HI) reductant.[51, 52] Raman spectra (Figure 3a) show an increase of the I(D)/I(G) intensity ratio, which confirms the reduction of the GO and the presence of more defects generated by the increase of the HI treatment time. That is because the removal of the oxygen-contained functional groups usually leave defects at the original locations and that can be reflected in the Raman signals.[10] The I(D)/I(G) ratio increases rapidly during the first 30 s (1.27 to 1.53) and slows down afterwards (1.53 to 1.55), showing an overall “fast-slow” reduction process. The XPS results (Figure 3b, c) further confirm the progress of the removal of the functional groups experiencing this type of process. The increase of C/O ratios and the weakened peaks of oxide-contained groups indicate that hydroxyl and epoxy groups are significantly reduced during the first 30 s, and reach lower contents when the time of the treatment is prolonged (60 s).

Damping Properties. The effect of the designed damping core layer on the energy dissipation of the beams has been evaluated using dynamic mechanical analysis (DMA) under temperature and frequency sweeps. Both storage modulus and loss factors (tan δ) of the samples before and after

only coating PU constrained layers remain no obvious difference (Figure 3d-g). The storage modulus of samples with GnPs core layer (Figure 3d, f) decreases in comparison to virgin PU, which may be ascribed to the relatively slips between flat graphene nanoplates. The storage modulus further decreases after GnPs oxidization, which may be due to the soft and wrinkled GO nanoplates that less contribute to the modulus of the beams than the stiff and flat GnPs. For samples with reduced GO (rGO), their storage modulus however increases and larger enhancements are achieved with the reduction time increasing (although the storage modulus of samples after 60 s reduction is still lower than that of samples with GnPs). On the contrary, the loss factors (tan δ) of samples with GnPs (Figure 3e, g) initially increases by 7% at glass transition (T_g) and 40% at room temperature (*RT,* 1 Hz) due to the interlaminar friction of GnPs in comparison to virgin PU. The tan δ is enhanced by 11% at T_g and 70% at *RT* owing to the introduction of wrinkles on graphene after oxidization, and picks up further to reach enhancements of 21% at T_g and 94% at *RT* for samples after 60 s reduction compared with pristine PU beams. Quasi-static energy dissipation properties (Figure 3h, Data processing in the Supporting Information) show that the energy dissipation coefficient (η) of samples with GnPs increases by 4% compared to the baseline PU beams, 30% due to the introduction of wrinkles in graphene nanoplates, and further reach 71% for samples with 60 s reduction. The increasing η is in agreement with the variation trend of tan δ, and both of them show a "fast-slow" increasing trend versus the HI treatment times, which is consistent with the removal process of functional groups as elucidated from the Raman and XPS analyses. Importantly, the loss factors (tan δ, 0.10~0.25) and storage modulus (*E'*, 150~300 MPa) from the DMA at 1 Hz (*RT*) are a touch higher than the energy dissipation coefficients (η, 0.07~0.15) and Young's modulus (*E*, 100~160 MPa) in quasi-static tests (Figure 3i), respectively. This confirms the consistency of our measurements.

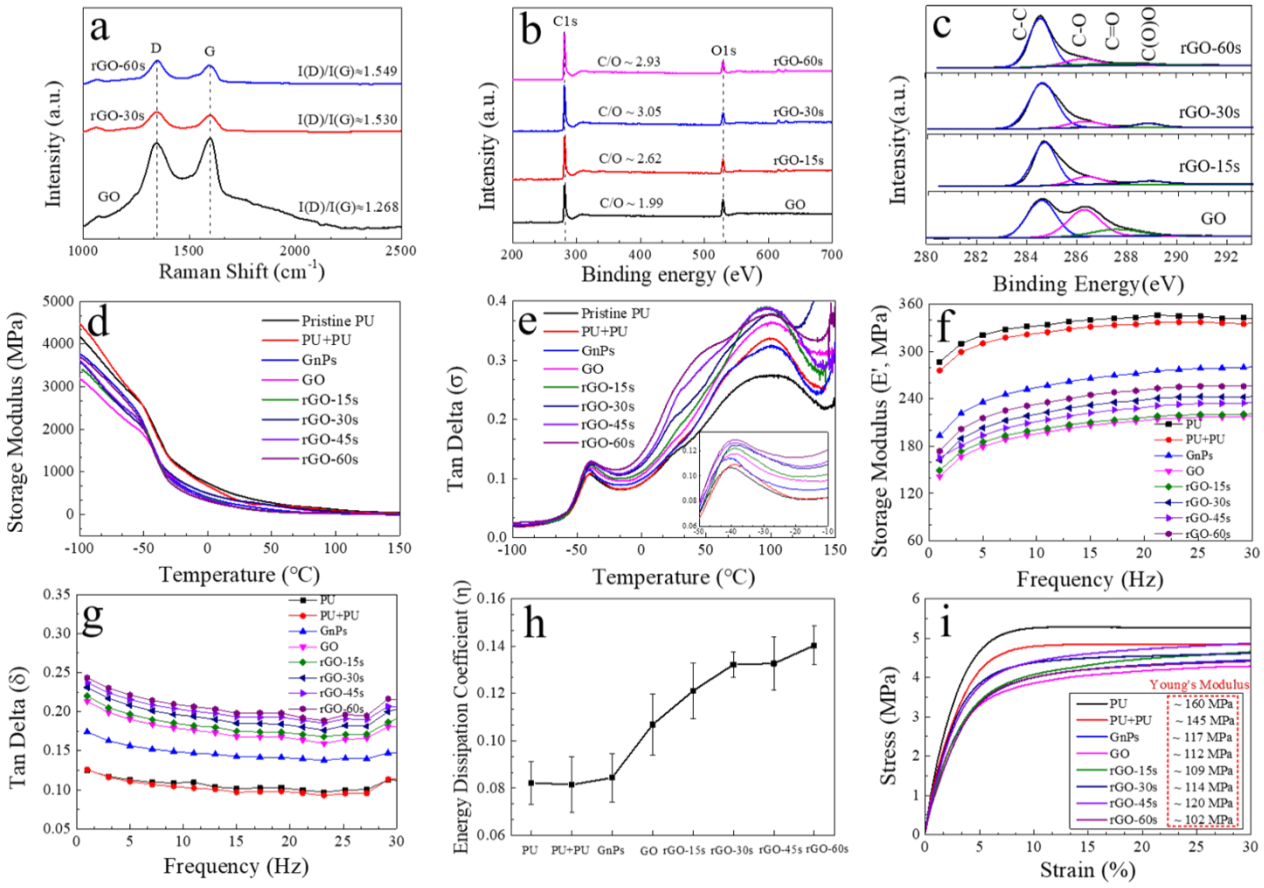

Figure 3. a) Raman spectra of GO and rGO with different reduction time. b) XPS full spectrums of GO (rGO) and c) their C1 spectrums. Dynamic damping properties as storage modulus and tan δ obtained by the DMA under d-e) frequency sweep (1-30 Hz) at *RT* and f-g) temperatures sweep (-100-150 °C) at 1 Hz. h) Quasi-static energy dissipation properties obtained from quasi-static three-point bending cycle tests. i) Stress-strain curves under uniaxial tension tests and their corresponding Young's Modulus derived from the slopes within the linear elastic range at 2%~3% strain.

Damping Mechanisms. To explore in depth the damping mechanism under frictional behavior, we have measured the friction forces of GnPs and GO nanoplates by AFM under Lateral Force Mode (see the details in the Supporting Information). The force profile patterns (Figure 4c) derived from the line 1 traced in the force image (Figure 4b) show that the force variations are in both trace and retrace modes, which are typical of mirror symmetry.[1] The friction forces of the GnPs feature a more stable pattern because of their smooth surfaces and are smaller than those produced in GO

nanoplates, even when measured on flat areas. This is due to the oxygen-contained groups that strengthen the out-of-plane elastic characteristics of the GO, with larger deformation being caused during the slips.[53] In contrast, large friction forces of the GO occur at the wrinkle sites whereas little evident friction is observed on the flat areas. The friction forces measured along the scanning direction present large values ("ridge") on the face side of the wrinkles, and small values ("valley") on the back side (Figure 4c, e, f). This behavior can be explained by the nature of stick-slip phenomena: the probe moving forwards is stuck by the puckered wrinkles and hence results in the increased friction force, then suddenly slips and causes the minor force when the wrinkles are overcome.[15] Some published articles have reported that the layers of GO sheets affect the friction force, with fewer layers providing larger friction.[54] Our work shows that the friction forces provided by three layered GO nanoplates are indeed ~1 nN higher than those of 7(10) layered GO nanoplates (Figure 4d). Those different forces are however one order of magnitude smaller compared with the ones measured in the wrinkles (10~20 nN) and therefore can be ignored during the analysis. In short, the wrinkles mainly contribute to the overall friction of the graphene sheets that provide topological mechanical barriers and cause the majority of the energy dissipation when the GO nanoplates are experiencing a mutual slip.

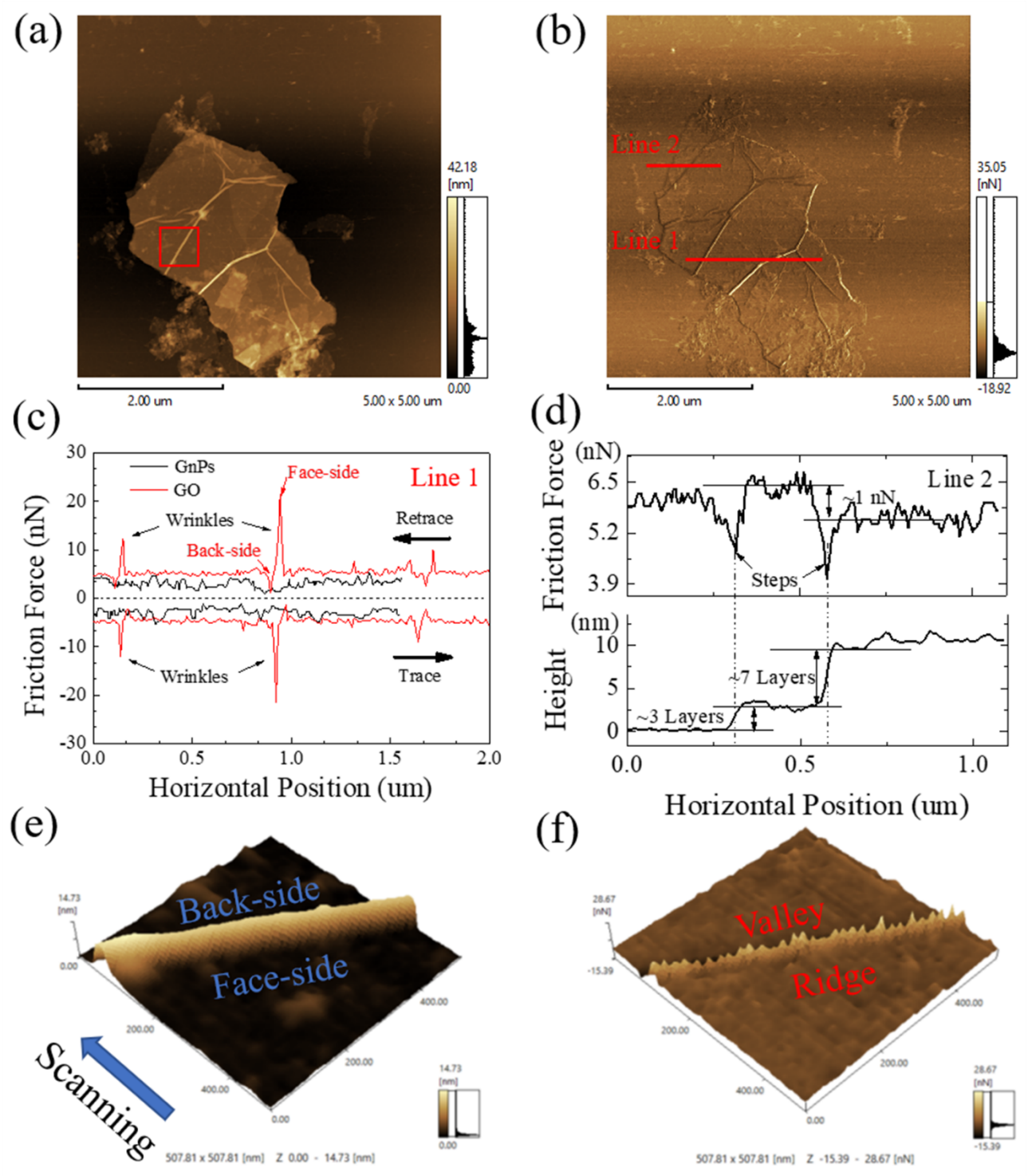

Figure 4. a) Scanning probe GO morphology and b) corresponding friction force image measured simultaneously by AFM under Lateral Force Mode (LFM). The high spot lines on the GO nanoplates are the ridgy wrinkles and their corresponding high friction force. c) Friction force profile patterns derived from GnPs force image and line 1 in image b). The ultra-high friction forces are located at the wrinkle areas. d) Friction force profile pattern and its corresponding height profile pattern derived from line 2 in image b). e) The morphology of a wrinkle and f) its 3D displayed force

image.

At this point let us discuss the damping mechanism observed in the sandwich nanobeams. The wrinkled GO nanoplates are overlapped to form the core layer, and the GO close to the PU phase are connected to the matrix with strong chemical bonds formed by the silicane coupling. When the beams are subjected to external bending, the outer constrained PU shells induce a shear load transfer on the inner PU phases, and their interfaces slide with a relative motion to match the deformation.[55] In this sense, the GO nanoplates close to PU matrix move together with the matrix, the inner interfacial slips of overlapped GO nanoplates are activated under the shear effect and contribute to the global damping properties of the structure. The results of the *in-situ* SEM under tensile loading identify the existence of this interface slip (Figure 5a-c). The interfacial friction mechanism of the wrinkled GO nanoplates starts at Point 2 and gradually ends when reaching Point 3. The main slip is provided by the shift of the interface within a 0.6%~2.0% strain range and the applied damping strain is ~1%, which well locates within this area. The existing wrinkles play the main interactions while the GO nanoplates slip in relative motion (Figure 5d). As a result of the random orientation of the wrinkles, one can observe the presence of three types of interaction motions: (1) parallel between wrinkles, (2) wrinkle-flat GO and (3) transverse between wrinkles. All these interactions could cause severe distortion of the wrinkles due to the large friction forces involved and present high energy dissipation under the mutual slip of GO nanoplates. As the applied strain increases, no further obvious interfacial slip is observed, and this may result from the self-locking of the wrinkled GO nanoplates due to the presence of large numbers of interactions between wrinkles. Cracks initially generate in the PU matrix (Point 5) and propagate to the interfaces (Point 6), this indicates that the GO core layers provide an additional and beneficial effect

as a reinforced transitional phase of the PU interfaces at a large applied strain. Here the 0.6%~2.0% strain range is termed as a 'functional zone'. Once an applied strain is in this zone, the interfacial slip mechanism of wrinkled GO nanoplates is activated, if lower than 0.6%, the shear force of the interface is not enough to drive the slip, and if beyond 2.0%, the self-locking of wrinkled GO nanoplates ends the slip.

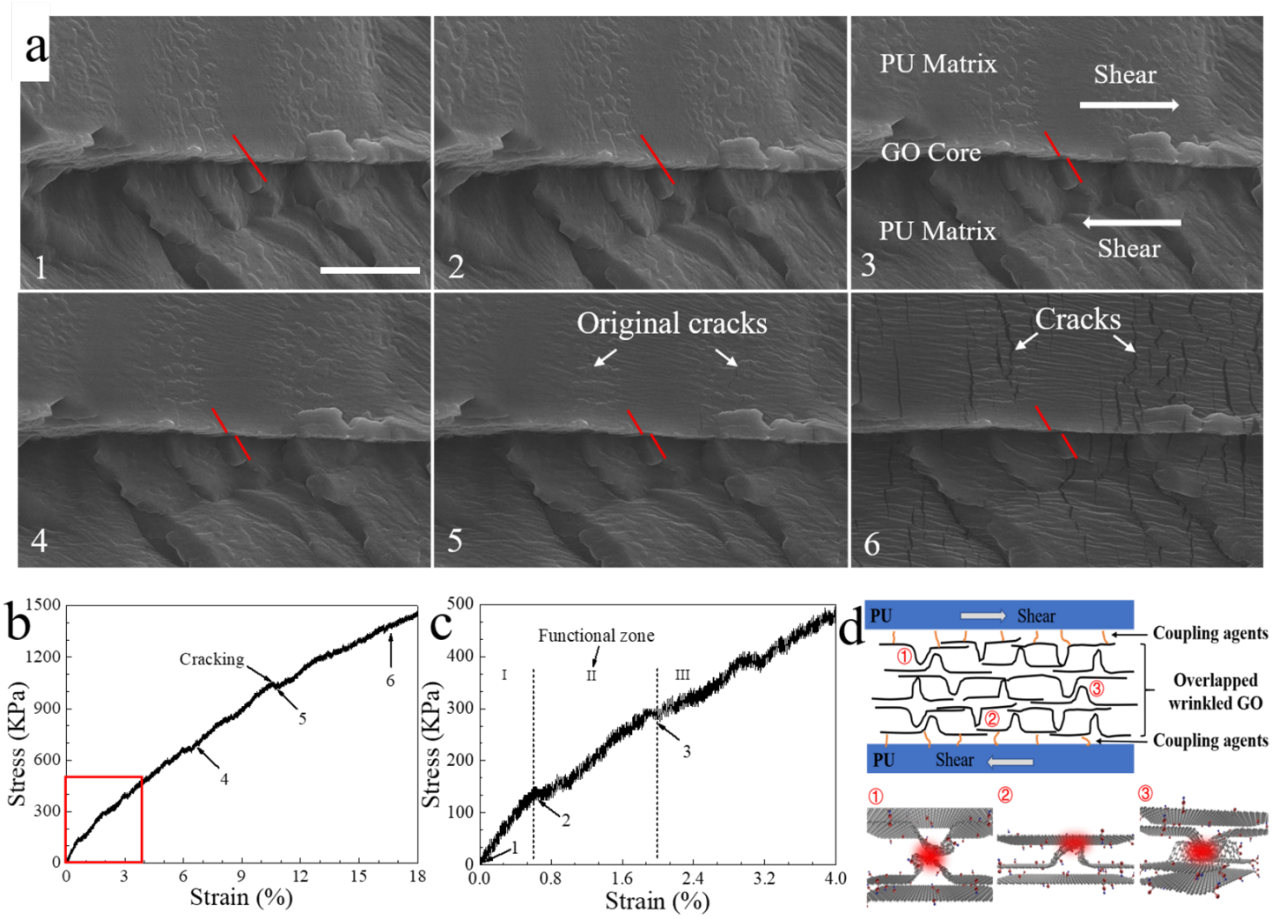

Figure 5. The mechanism of the interfacial slip observed under *in-situ* tension SEM. a) The evolution of the interfacial slip marked as the shift of red line, scale bar: 20 μm. b) The corresponding stress-strain curves and c) the enlarged graph. d) Schematic illustrating the energy dissipation mechanism of interlaminar slips of wrinkled GO nanoplates. Three main motions between wrinkles are present: (1) parallel between wrinkles, (2) wrinkle-flat GO, and (3) transverse between wrinkles. (Just shown the top sheets of GO nanoplates here)

How the GO Reduction Affects the Damping Mechanism. We have ascertained that the wrinkles mainly contribute to damping, hence they are chosen to probe how they impact the damping mechanism. Yang *et al.* has clarified that the reduction process can induce crumples on rGO nanoplates,[56] the almost indistinguishable morphologies of the GOs before and after reduction in our work however indicate that the reduction process does not contribute to the formation of wrinkles on the coated GO nanoplates (Figure S6 in the Supporting Information). The GO nanoplates presented are chemically coated on the PU surface because of the coupling agent, and this may be the reason for inhibiting their puckering. The COFs of the wrinkles are increased with the increase of their orientation angle (Figure 6a). This relationship has been also observed in Long and coworker's work, whereby the anisotropy of COFs reaches as high as ~194%, and it is attributed to more deformation of the graphene produced when probing along a perpendicular direction to the ripple lines.[15] The observed wrinkled GO-GO slip behavior presents however isotropic characteristics when considering the whole amount of GO nanoplates. Most importantly, the COFs of the identified wrinkles present a growth trend with the reduction time prolonging, and a 7.80% increase achieved after 60 s.

To investigate the underlying mechanism of the increased COFs, we have considered the size of the wrinkles firstly. The results show that the wrinkles shrink as the reduction process narrows their width and increases their height (Figure 6b, d-f). According to Lerf-Klinowski's GO model, the basal planes of GO sheets are mainly functionalized by hydroxyl and epoxy groups and the edges by carboxylic and hydroxyl groups.[57] The groups present in the basal planes significantly contribute to the interlayer distance in GO nanoplates.[58] The XPS results (Figure 3c) confirm that the epoxy, hydroxyl and keto groups are the main groups attached on GO and the reduction process leads to the decrease of the groups. The XRD results (Figure 6c) show a characteristic peak for the GO at

about 9.7°, which corresponds to an interlayer spacing of 9.2 Å attributed to the existence of large numbers of oxidative groups. The restacking of the rGO sheets caused by the removal of the basal plane groups leads to the appearance of the (002) diffraction peaks (~23.7°, *d*-spacing = 3.8 Å), and the peaks become stronger since more groups are eliminated with the reduction time increasing. The smaller diffraction peak angles and broader spans are an indicative of a disordered stacking resulting from the highly wrinkled graphene sheets compared with the sharp characteristic peak of GnPs (~26.5°, *d*-spacing = 3.5 Å). The increased interlaminar force (*i.e.* Van der Waals force) of the rGO nanoplates ascribing to the decreased interlayer spacing distance (from 9.2 Å to 3.8 Å) is the driving factor behind the shrinking of the wrinkles (see the inserted schematic in Figure 6b). It has been proved by both Tripathi and Ye's works that the higher wrinkles yield larger friction as the higher bending flexibilities and tractions would be triggered while the probe tip is scanning over the wrinkles.[30, 31] Moreover, the introduction of defects (vacancies) proved by the Raman analysis can reduce the stiffness of GO nanoplates.[59] The shrunken and more flexible wrinkles resulted from GO reduction therefore conspire to produce a larger deformation near the contact edge, and also an increased effective contact area, which leads to an enhanced friction behavior of the wrinkles.[10, 30, 31, 59]

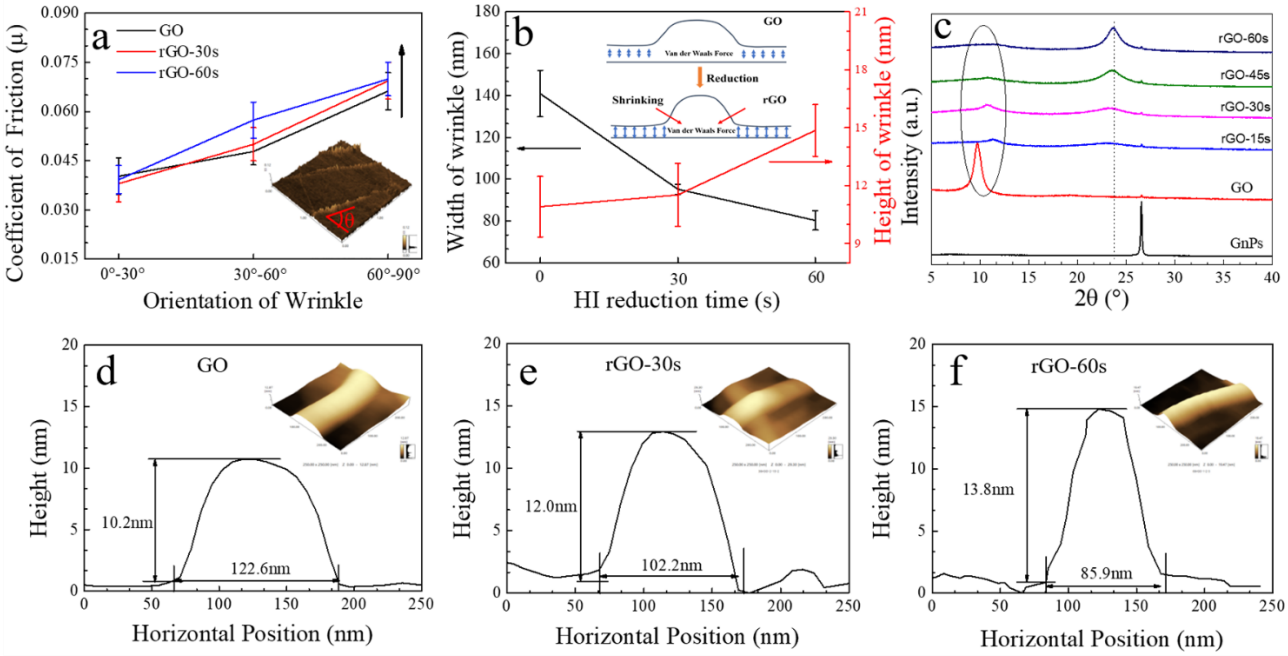

Figure 6. a) COFs of the wrinkles under different orientations and their HI reduction times. b) The variation of the wrinkle size as a function of the reduction time and the visualized shrinking process of a wrinkle (inserted graph). c) XRD patterns of rGO coatings collected under different reduction times. d-f) Cross-section diagrams of the wrinkles derived from the morphology images and their corresponding 3D display (inserted) under different reduction times (0 s, 30 s, 60 s).

The viscosity and adhesive forces are also considered and measured by AFM under Force Modulation Mode and Force Curve Mode (see the details in the Supporting Information). The viscoelasticity (magnitude and phase images) of the wrinkled GO nanoplates (Figure 7a, b) shows that the wrinkles present larger viscoelastic effects than flat areas. Along the scanning direction (from right to left) a large elasticity is observed on the face side of the wrinkles and a large viscosity on the back side, resulted from the scanning mode of “uphill” on the face side and “downhill” on the back side. The elasticity of the wrinkles decreases while the viscosity increases with the increase of the HI treatment time (Figure 7c). In addition, the larger adhesive forces are obtained in the wrinkles compared to flat areas (Figure 7d-f). That is because the ridge-like wrinkles present higher

bending flexibilities and tractions than the flat areas of graphene when the probe tips approach and release the graphene surfaces.[30] The results also show that the adhesive force in the wrinkles increases as the GO reduction time increases. The main reason behind this is the introduction of defects caused by the reduction process, which makes wrinkles softer.[30, 59] This matches well with the observed decreased elasticity of the wrinkles, and also justifies the increase of viscosity and the adhesive force. To explain the strengthened interactions between the wrinkles, they can be identified as interactions between the GO-GO interfaces. The basal plane oxygen functional groups (hydroxy and epoxy) generate high repulsive electrostatic forces that lead to low interfacial friction.[7] As fewer functional groups are left with the increase of the reduction time, the reduced interlayer distance and repulsive forces are conducive to stronger Van der Waals forces and electrostatic attractions, which result in an increase of the equivalent viscosity and the adhesive forces exerted by the wrinkles.[6] In conclusion, both the increased effective contact area and adhesive force (viscosity) contribute to the enhancement of the friction force between the wrinkles, and thus to higher energy dissipation and damping properties of the nanocomposites (Figure S7 in the Supporting Information).

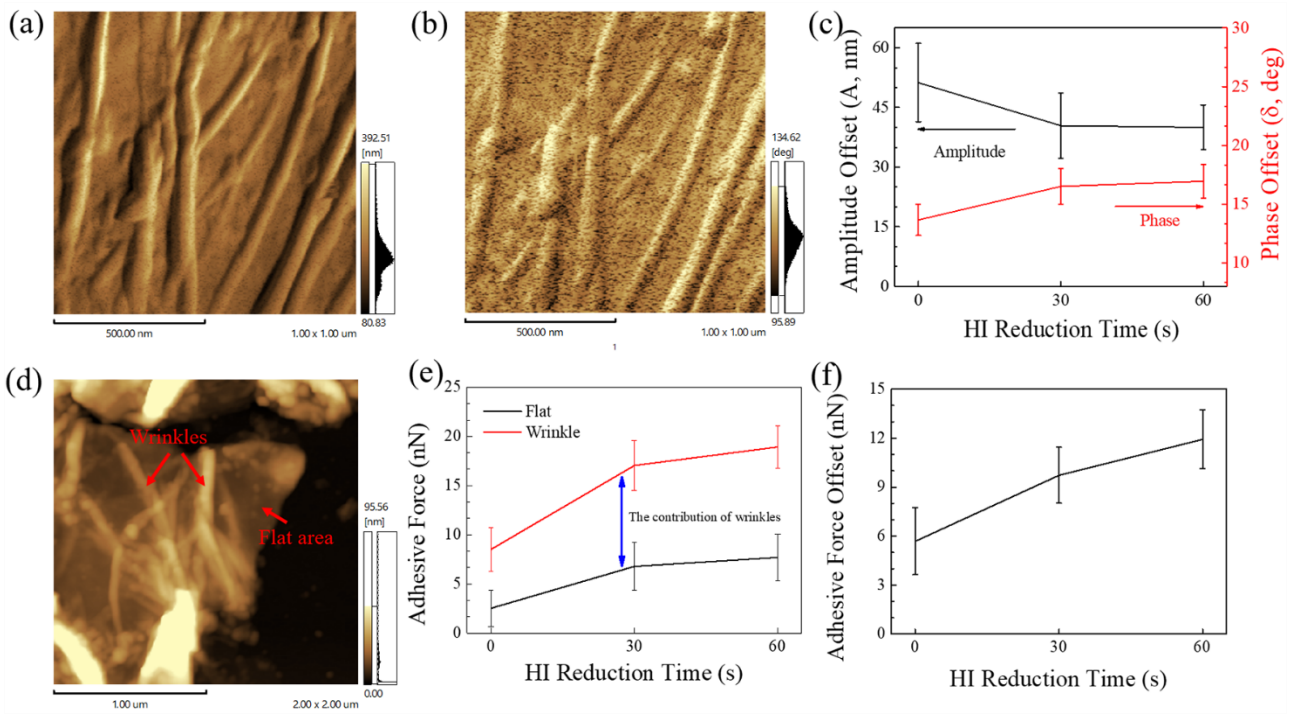

Figure 7. a) Elasticity (amplitude) and b) viscosity (phase) images of a wrinkled GO nanoplate. c) The viscoelasticity of the wrinkles as a function of the HI reduction time. d) A wrinkled GO shown with wrinkles and flat areas, and e) their adhesive forces as function of the HI reduction time. f) The contribution of the wrinkles adhesive force derived from the difference between wrinkles and flat areas values.

Further Discussion in Context. Damping properties of the present polyurethane-based graphene nanocomposites compared with results from open literatures are summarized in Table 1. In general, traditional graphene (oxide) nanocomposites with distributed nanofillers show a limited enhancement (less than 10%), or even a decrease in terms of damping properties. An accepted explanation for this behavior is the non-uniform dispersion of the fillers proposed, as the re-aggregation and self-scrolling of the graphene sheets in nanocomposites limit their high surface area advantage.[40, 60, 61] A second explanation is related to the strong interface bonds between chemically modified graphene and the matrix, enhancing the load transfer and restricting the graphene-matrix interfacial slip mechanism.[47-49] The last accepted explanation is about the

confinement of the polymeric chains between the graphene particles, which inhibits the natural damping performance of the polymer matrix.[44] Remarkably, the damping properties of the composites with rGO content as low as ~0.08wt% in this work provide a very unusual enhancement of 94% by introducing the interfacial friction mechanism presenting in wrinkled rGO-rGOs. The dip-coated GO nanoplates are in an unfolded and overlapped form that possess large surface area, and the interfacial friction mechanism of the GO nanoplates can be triggered in an easier way under the sandwich structure configuration of the nanobeams. The introduced wrinkles play the main role in enhancing the damping, with the wrinkled GO-based nanocomposites by dissipating 75% more energy compared with the nanocomposites with GnPs. The size, viscoelasticity and adhesive force of the wrinkles can be engineered by GO reduction to adjust the COFs. With COFs of the wrinkles only enhanced by 7.8%, the damping of rGO-based composites is however further increased by 34% due to the accumulation of energy dissipation within the weight fraction of the rGO nanoplates. It is also worth pointing out that by tailoring the dispersion of extremely low contents of engineered graphene particles in polyurethane, our work provides valuable indications on how to significantly increase the damping of nanocomposites in an environment - room temperature (under different frequency) - that is relevant to many technological applications.

Table 1. Damping properties of present composite material compared with reported results

Composites	Content	Enhancement	Reference
PU/rGO	0.5wt%	~4% (*Tg*[a)], 10 Hz)	Yu et al.[62]
PU/GO	1.0wt%	~7% (*Tg*, 1 Hz)	Shamsi et al.[63]
PU/GnPs	0.5wt%	~6% (T_g, 1 Hz)	Aida et al.[64]
PU/GnPs	0.5wt%	~2% (T_g, 10 Hz)	Samsook et al.[65]
PU/rGO	2.0wt%	Decrease (T_g, 1 Hz)	Chen et al.[49]
PU/G nanoribbons	series	Decrease (T_g, 1 Hz)	Xiang et al.[48]
PU/Graphene	2.0wt%	Decrease (T_g, 1 Hz)	Pokharel et al.[47]
PU/GnPs	~0.08wt%	7% (T_g[a)], 1 Hz)	Our work
PU/GO	~0.08wt%	11% (T_g, 1 Hz)	
PU/rGO	~0.08wt%	21% (T_g, 1 Hz)	
PU/GnPs	~0.08wt%	40% (*RT*[b)], 1 Hz)	
PU/GO	~0.08wt%	70% (*RT*, 1 Hz)	
PU/rGO	~0.08wt%	94% (*RT*, 1 Hz)	

[a)] T_g: glass transition temperature (~ -42 ℃); [b)] *RT*: room temperature (under frequency sweep).

CONCLUSIONS

In the work, sandwich structure beams with unfolded and overlapped GO (rGO) nanoplates as the core layers are designed and successfully fabricated by dip-coating method. The damping properties of composites are both investigated under quasi-static and dynamic states. By capitalizing on the damping mechanism of GO-GO interfacial slips, wrinkles are confirmed to play a pivotal role in energy dissipation due to their large coefficients of friction. We demonstrate that the damping performance after GO reduction is further enhanced resulted from the increased effective contact area and adhesive force of wrinkles. rGO-contained nanocomposites, featured with sandwich

structures, afford higher damping properties under the damping mechanism of interface slips of wrinkled rGO nanoplates compared with traditional distributed nanocomposites. This work provides an in-depth understanding of the structural mechanism for establishing the design protocol of nanocomposites for damping applications. Yielded by the dip-coating process merely repeated once, the composites reveal such high enhanced damping capabilities (94%). It is reasonable to predict that the damping performance will be further enhanced as more rGO core layers are introduced in the matrix by further repeating the dip-coating process. Relevant works are under way.

METHODS

Preparation of Dip-Coating Ink. Graphite flakes (3.6 g, particle size≤30 μm) were expanded using a solution of $K_2S_2O_4$ (3 g) and P_2O_5 (3 g) in concentrated H_2SO_4 (15 ml) at 80 °C for 72 h. After 2 h ultrasonication, the solution was carefully poured into water before being filtered through a 0.45 μm PTFE filter and washed thoroughly with water three times, then dried in an oven at 50 °C for 48 h, the GnPs powders were obtained. GO was produced using a modified Hummer's method from GnPs.[66] GnPs (2.00 g), $NaNO_3$ (1.00 g) and H_2SO_4 (46 mL) were first mixed together in a three-neck beaker which was kept in an ice bath whilst being stirred. After 30 min, $KMnO_4$ (6 g) were added to the suspension stepwise kept reacting for 2 h. Then the suspension was heated to 35 ℃ and held for 3 h. Distilled water (46 mL) was slowly poured into the beaker and the temperature quickly reached 98 ℃. After maintaining 10 min, another distilled water (100 mL) and H_2O_2 (36 mL, 30%) were slowly added to cease the reaction. For purification, HCl (53 mL, 36%) was needed and the suspension was washed by deionized water several times with the assistance of centrifugation. The washed suspension was condensed in an oven (50 ℃) for 60 h to yield dried GO

membrane, followed by grounding into powders. Finally, the GnPs and GO powders were re-dissolved in ethylene glycol with ultrasonication (3 h) and agitation (12 h) at room temperature, an ink of 0.4wt% solution was produced for dip-coating process. All reagents were purchased from Sinopharm Chemical Reagent Co. Ltd and used as received without further purification.

Preparation of Sandwich Structure Nanobeams. The pristine PU beams were first fabricated using a water-based aliphatic polyurethane dispersion (PUD, 715) from Jining Huakai Resin Co. Ltd, China. In order to build strong chemical bonds between PU and GO (GnPs), PU beams were treated by O_2 plasma, and silicane coupling agents (KH-550) were added into the ink. In addition, acetic acid was added and the pH of ink solution was kept in 3.5, which can accelerate the hydrolysis of coupling agent. Then PU beams were immersed in the ink and taken out 10 min later to dry at 50 °C for 40 h. For GO reduction, the GO coated beams were immersed fully in HI solution (45%) and allowed to proceed at 80 °C for 15 s, 30 s, 45 s, 60 s, respectively, which resulted in the different reduction degree of GO nanoplates. Then alternately rinsed with deionized water and alcohol three times, dried at 50 ℃ for 2 h. Following the similar dip-coating process, PUD was used again to seal the GO or rGO coating as a top coating.

(*In-Situ*) SEM Measurements. Surface morphologies were investigated by a cold Field Emission Scanning Electron Microscopy (FE-SEM, Hitachi S-4800) operating at 3.0 kV. The *in-situ* tension of samples was realized by a Scanning Electron Microscopy (SEM, Quanta650) equipped with a homemade tensile stage. Before observation, the samples were sprayed with Au for 90 s.

Characterization of Lateral Force, Viscoelasticity and Adhesive Force. Scanning probe images of GO (rGO) morphologies and friction force images were simultaneously measured under the Lateral Force Mode (LFM) with a Scanning Probe Microscope (SPM-9700, SHIMADZU). In addition, Force Modulation Mode (FMM) and Force Curve Mode (FCM) were employed to

characterize the viscoelasticity and adhesive force of wrinkled GO (rGO) nanoplates. All the measurements were conducted at room temperature.

Raman, XPS, XRD and Contact Angle Measurements. Raman spectrum registered on a DXR Smart Raman spectrometer (irradiation wavelength: 532 nm) and X-ray photoelectron spectroscopy (XPS) equipment supplied by Kratos Analytical Ltd were employed to analyze the precise process of GO reduction and the progress of removing oxygen-contained functional groups. The X-Ray Diffraction (XRD Empyrean 200895 PANalytical B.V.) was used to define the lamellar distance of GO sheets. The GO coatings were dried in an oven under 50 °C more than 40 h, so as to eliminate the influence of solvent. The contact angles of GO and rGO coatings were measured by Contact Angle Meter (DCA20) under room temperature.

Measurement of Mechanical Properties. Tension tests were performed at room temperature by using Zwick/Roell Z5.0 universal testing machine with 5kN load cell. Tests were taken under stroke control with a maximum strain of 18% at a crosshead speed of 3 mm min^{-1}. Quasi-static three-point bending cyclic tests were performed by INSTRON 5943 universal testing machine with 1kN load cell. Tests were taken under stroke control with a maximum strain of 10% at a crosshead speed of 5 mm min^{-1} under the standard measurement of ASTM D790.

Characterization of Dynamic Damping Properties. The dynamic damping properties as both frequency and temperature dependent viscoelastic properties (storage modulus *E'* and tan δ) of the designed composites were evaluated by Dynamic Mechanical Analyzer (DMA, TAQ800). The specimens were subjected to a frequency scan of 1 Hz~30 Hz at room temperature and a temperature scan of -100~150 ℃ with fixed frequency of 1 Hz under dual cantilever mode, the amplitudes were setting 40 μm (~1% deformation).

Conflict of Interest: The authors declare no competing financial interest.

Acknowledgement. FXQ would like to thank the financial support of NSFC No. 51671171 and No. 51601168; Fundamental Research Funds for the Central Universities No. 2018QNA4001 and 'National Youth Thousand Talent Program' of China. The authors would like to thank the laboratory technician Li Xu who has given lots of helps in the DMA measurements, and we also appreciate constructive and insightful advice from Prof. Rod Ruoff of Ulsan National Institute of Science and Technology in South Korea.

Supporting Information Available: This material is available free of charge *via* the Internet at http://pubs.acs.org.

SEM images of samples coated with GnPs and GO; a table of some properties of common solvents related to the GO solubility; visual images of GO ink with and without coupling agent treatment after 48 h quiescence; cross-section images of free-standing GO coating membranes; *in-situ* SEM images under tensile loading and the morphologies of exfoliated PU phases; contact angles of rGO coatings as a function of GO reduction time; SEM images of GO coating before and after 30 s HI treatment; mechanism break-down schematic detailing how the reduction process of wrinkled GO nanoplates affecting the energy dissipation of their interlaminar slip; and data processing for quasi-static three-point bending cycle tests performed by INSTRON 5943 universal testing machine and force measurements by Atomic Force Microscope including Lateral Force Mode, Force Modulation Mode and Force Curve Mode.

REFERENCES

(1) Lang, H.; Peng, Y.; Zeng, X. Effect of Interlayer Bonding Strength and Bending Stiffness on 2-Dimensional Materials' Frictional Properties at Atomic-Scale Steps. *Appl. Surf. Sci.* **2017,** *411*, 261-270.

(2) Feng, X.; Kwon, S.; Park, J. Y.; Salmeron, M. Superlubric Sliding of Graphene Nanoflakes on Graphene. *Acs Nano* **2013,** *7* (2), 1718-1724.

(3) Berman, D.; Erdemir, A.; Sumant, A. V. Approaches for Achieving Superlubricity in Two-Dimensional Materials. *Acs Nano* **2018,** *12* (3), 2122-2137.

(4) Kawai, S.; Benassi, A.; Gnecco, E.; Söde, H.; Pawlak, R.; Feng, X.; Müllen, K.; Passerone, D.; Pignedoli, C. A.; Ruffieux, P. Superlubricity of Graphene Nanoribbons on Gold Surfaces. *Science* **2016,** *351* (6276), 957-961.

(5) Liu, Y.; Song, A.; Xu, Z.; Zong, R.; Zhang, J.; Yang, W.; Wang, R.; Hu, Y.; Luo, J.; Ma, T. Interlayer Friction and Superlubricity in Single-Crystalline Contact Enabled by Two-Dimensional Flake-Wrapped Atomic Force Microscope Tips. *ACS Nano* **2018,** *12* (8), 7638-7646.

(6) Wang, L. F.; Ma, T. B.; Hu, Y. Z.; Wang, H.; Shao, T. M. Ab Initio Study of the Friction Mechanism of Fluorographene and Graphane. *Journal of Physical Chemistry C* **2013,** *117* (24), 12520-12525.

(7) Bhowmick, S.; Sen, F. G.; Banerji, A.; Alpas, A. T. Friction and Adhesion of Fluorine Containing Hydrophobic Hydrogenated Diamond-like Carbon (F-H-DLC) Coating Against Magnesium Alloy AZ91. *Surf. Coat. Technol.* **2015,** *267*, 21-31.

(8) Van Wijk, M. M.; Dienwiebel, M.; Frenken, J. W. M.; Fasolino, A. Superlubric to Stick-Slip Sliding of Incommensurate Graphene Flakes on Graphite. *Physical Review B Condensed Matter* **2015,** *88* (23), 235423-235430.

(9) Sun, X. Y.; Wu, R. N.; Xia, R.; Chu, X. H.; Xu, Y. J. Effects of Stone-Wales and Vacancy Defects in Atomic-Scale Friction on Defective Graphite. *Appl. Phys. Lett.* **2014,** *104* (18), 183109-183113.

(10) Gajurel, P.; Kim, M.; Wang, Q.; Dai, W.; Liu, H.; Cen, C. Vacancy-Controlled Contact Friction

in Graphene. *Adv. Funct. Mater.* **2017**, *27*(47), 1702832-1702840.

(11) Dong, Y.; Wu, X.; Martini, A. Atomic Roughness Enhanced Friction on Hydrogenated Graphene. *Nanotechnology* **2013,** *24* (37), 375701-375707.

(12) Dong, Y.; Liu, X. Z.; Egberts, P.; Ye, Z.; Carpick, R. W.; Martini, A. Correlation Between Probe Shape and Atomic Friction Peaks at Graphite Step Edges. *Tribology Letters* **2013,** *50* (1), 49-57.

(13) Kim, D.-I.; Park, S.-M.; Hong, S. W.; Jeong, M. Y.; Kim, K. H. The Periodicity in Interfacial Friction of Graphene. *Carbon* **2015,** *85*, 328-334.

(14) Choi, J. S.; Kim, J. S.; Byun, I. S.; Lee, D. H.; Lee, M. J.; Park, B. H.; Lee, C.; Yoon, D.; Cheong, H.; Lee, K. H. Friction Anisotropy-Driven Domain Imaging on Exfoliated Monolayer Graphene. *Science* **2011,** *333* (6042), 607-10.

(15) Long, F.; Yasaei, P.; Yao, W.; Salehi-Khojin, A.; Shahbazian-Yassar, R. Anisotropic Friction of Wrinkled Graphene Grown by Chemical Vapor Deposition. *Acs Applied Materials & Interfaces* **2017,** *9* (24), 20922-20927.

(16) Wang, J.; Wang, F.; Li, J.; Wang, S.; Song, Y.; Sun, Q.; Jia, Y. Theoretical Study of Superlow Friction Between Two Single-Side Hydrogenated Graphene Sheets. *Tribology Letters* **2012,** *48* (2), 255-261.

(17) Wang, J.; Li, J.; Fang, L.; Sun, Q.; Jia, Y. Charge Distribution View: Large Difference in Friction Performance Between Graphene and Hydrogenated Graphene Systems. *Tribology Letters* **2014,** *55* (3), 405-412.

(18) Sen, F. G.; Qi, Y.; Alpas, A. T. Tribology of Fluorinated Diamond-Like Carbon Coatings: First Principles Calculations and Sliding Experiments. *Lubr. Sci.* **2013,** *25* (2), 111-121.

(19) Zeng, X.; Peng, Y.; Lang, H. A Novel Approach to Decrease Friction of Graphene. *Carbon*

2017, *118*, 233-240.

(20) Tang, J.; Zhou, H.; Liang, Y.; Shi, X.; Yang, X.; Zhang, J. Properties of Graphene Oxide/Epoxy Resin Composites. *Journal of Nanomaterials* **2014,** *2014* (2), 696859-696864.

(21) Li, B.; Olson, E.; Perugini, A.; Zhong, W. H. Simultaneous Enhancements in Damping and Static Dissipation Capability of Polyetherimide Composites with Organosilane Surface Modified Graphene Nanoplatelets. *Polymer* **2011,** *52* (24), 5606-5614.

(22) Suhr, J.; Koratkar, N. A. Energy Dissipation in Carbon Nanotube Composites: A Review. *Journal of Materials Science* **2008,** *43* (13), 4370-4382.

(23) Zhang, X. C.; Peng, H. X.; Limmack, A. P.; Scarpa, F. Viscoelastic Damping Behaviour of Cup Stacked Carbon Nanotube Modified Epoxy Nanocomposites with Tailored Interfacial Condition and Re-agglomeration. *Compos. Sci. Technol.* **2014,** *105*, 66-72.

(24) Zhang, H.; Guo, Z.; Gao, H.; Chang, T. Stiffness-Dependent Interlayer Friction of Graphene. *Carbon* **2015,** *94*, 60-66.

(25) Sinclair, R. C.; Suter, J. L.; Coveney, P. V. Graphene–Graphene Interactions: Friction, Superlubricity, and Exfoliation. *Adv. Mater.* **2018**, *30*(13), 1705791-1705798.

(26) Deng, S.; Berry, V. Wrinkled, Rippled and Crumpled Graphene: An Overview of Formation Mechanism, Electronic Properties, and Applications. *Mater. Today* **2016,** *19* (4), 197-212.

(27) Zang, J.; Seunghwa, R.; Nicola, P.; Wang, Q.; Tu, Q.; Buehler, M. J.; Zhao, X. Multifunctionality and Control of the Crumpling and Unfolding of Large-Area Graphene. *Nature Materials* **2013,** *12* (4), 321-325.

(28) Rouby, W. M. A. E. Crumpled Graphene: Preparation and Applications. *Rsc Advances* **2015,** *5* (82), 66767-66796.

(29) Yu, C.; Ma, P.; Xi, Z.; Wang, A.; Tao, Q.; Wu, S.; Qiang, C. All-Solid-State Flexible

Supercapacitors Based on Highly Dispersed Polypyrrole Nanowire and Reduced Graphene Oxide Composites. *Acs Appl Mater Interfaces* **2014,** *6* (20), 17937-17943.

(30) Tripathi, M.; Awaja, F.; Bizao, R. A.; Signetti, S.; Iacob, E.; Paolicelli, G.; Valeri, S.; Dalton, A.; Pugno, N. M. Friction and Adhesion of Different Structural Defects of Graphene. *ACS Applied Materials & Interfaces* **2018,** *10* (51), 44614-44623.

(31) Ye, Z.; Tang, C.; Dong, Y.; Martini, A. Role of Wrinkle Height in Friction Variation with Number of Graphene Layers. *J. Appl. Phys.* **2012,** *112* (11), 116102-116105.

(32) Bae, J. Y.; Chung, D. J.; An, J. H.; Shin, D. H. Effect of the Structure of Chain Extenders on the Dynamic Mechanical Behaviour of Polyurethane. *Journal of Materials Science* **1999,** *34* (11), 2523-2527.

(33) Benjamin, S. An Overview of Constrained-Layer Damping Theory and Application. *J. Acoust. Soc. Am.* **2013,** *133* (5), 3332-3337.

(34) Cherkasov, V. D.; Yu, V. Y.; Avdonin, V. V. Damping Properties of Sandwich Beams with Viscoelastic Layer. *IOP Conference Series: Materials Science and Engineering* **2017,** *262* (1), 012024-012029.

(35) KohjiSuzuki; KazuroKageyama; IsaoKimpara; SanaeHotta; TakuoOzawa; ShigenoriKabashima; TsuyoshiOzaki. Vibration and Damping Prediction of Laminates with Constrained Viscoelastic Layers--Numerical Analysis by a Multilayer Higher-Order-Deformable Finite Element and Experimental Observations. *Mechanics of Composite Materials & Structures* **2003,** *10* (1), 43-75.

(36) Zhang, Y.; Geng, M.; Zhang, H.; He, Y.; Peng, C.; Huang, Q.; Fan, C. High-Conductivity Graphene Nanocomposite Via Facile, Covalent Linkage of Gold Nanoparticles to Graphene Oxide. *Chin. Sci. Bull.* **2012,** *57* (23), 3086-3092.

(37) Dai, J.; Wang, G.; Ma, L.; Wu, C. Study on the Surface Energies and Dispersibility of Graphene Oxide and Its Derivatives. *Journal of Materials Science* **2015,** *50* (11), 3895-3907.

(38) Hansen, C.; Poulsen, T. *Hansen Solubility Parameters — Biological Materials*. 2007.

(39) Li, D.; Müller, M. B.; Gilje, S.; Kaner, R. B.; Wallace, G. G. Processable Aqueous Dispersion of Graphene Nanosheets. *Nature Nanotechnology* **2008,** *3* (2), 101-105.

(40) Ma, W.; Li, J.; Deng, B.; Lin, X.; Zhao, X. Properties of Functionalized Graphene/Room Temperature Vulcanized Silicone Rubber Composites Prepared by an In-situ Reduction Method. *Journal of Wuhan University of Technology-Mater. Sci. Ed.* **2013,** *28* (1), 127-131.

(41) Xiao-Chong Zhang, F. S., Ronan McHale, Andrew P. Limmack; Peng, a. H.-X. Carbon Nano-Ink Coated Open Cell Polyurethane Foam with Micro-Architectured Multilayer Skeleton for Damping Applications. *RSC Advances* **2016**, *6*, 80334–80341.

(42) Liu, N.; Pan, Z.; Fu, L.; Zhang, C.; Dai, B.; Liu, Z. The Origin of Wrinkles on Transferred Graphene. *Nano Research* **2011,** *4* (10), 996-1004.

(43) Qin, H.; Sun, Y.; Liu, J. Z.; Liu, Y. Mechanical Properties of Wrinkled Graphene Generated by Topological Defects. *Carbon* **2016,** *108*, 204-214.

(44) Chen, B.; Ma, N.; Bai, X.; Zhang, H.; Zhang, Y. Effects of Graphene Oxide on Surface Energy, Mechanical, Damping and Thermal Properties of Ethylene-Propylene-Diene Rubber/Petroleum Resin Blends. *Rsc Advances* **2012,** *2* (11), 4683-4689.

(45) Chang, C.; Song, Z.; Lin, J.; Xu, Z. How Graphene Crumples Are Stabilized? *Rsc Advances* **2013,** *3* (8), 2720-2726.

(46) Chen, X.; Yi, C.; Ke, C. Bending Stiffness and Interlayer Shear Modulus of Few-Layer Graphene. *Appl. Phys. Lett.* **2015,** *106* (10), 490-495.

(47) Pokharel, P.; Pant, B.; Pokhrel, K.; Pant, H. R.; Lim, J. G.; Dai, S. L.; Kim, H. Y.; Choi, S.

Effects of Functional Groups on the Graphene Sheet for Improving the Thermomechanical Properties of Polyurethane Nanocomposites. *Composites Part B* **2015,** *78*, 192-201.

(48) Changsheng, X.; Cox, P. J.; Akos, K.; Bostjan, G.; Hashim, D. P.; Zheng, Y.; Zhiwei, P.; Chih-Chau, H.; Gedeng, R.; Samuel, E. L. G. Functionalized Low Defect Graphene Nanoribbons and Polyurethane Composite Film for Improved Gas Barrier and Mechanical Performances. *Acs Nano* **2013,** *7* (11), 10380-10386.

(49) Chen, Z.; Lu, H. Constructing Sacrificial Bonds and Hidden Lengths for Ductile Graphene/Polyurethane Elastomers with Improved Strength and Toughness. *J. Mater. Chem.* **2012,** *22* (25), 12479-12490.

(50) Cahangirov, S.; Ciraci, S.; Qzcelik, V. O. Superlubricity Through Graphene Multilayers Between Ni(111) Surfaces. *Physical Review B* **2013,** *87* (20), 1853-1865.

(51) Pei, S.; Zhao, J.; Du, J.; Ren, W.; Cheng, H.-M. Direct Reduction of Graphene Oxide Films into Highly Conductive and Flexible Graphene Films by Hydrohalic Acids. *Carbon* **2010,** *48* (15), 4466-4474.

(52) Coxon, J. M.; Townsend, M. A. E. Computational Study on the Ring-Opening Reaction of Protonated Oxirane and Methylpropene. *Tetrahedron* **2007,** *63* (25), 5665-5668.

(53) Ko, J. H.; Kwon, S.; Byun, I. S.; Jin, S. C.; Park, B. H.; Kim, Y. H.; Park, J. Y. Nanotribological Properties of Fluorinated, Hydrogenated, and Oxidized Graphenes. *Tribology Letters* **2013,** *50* (2), 137-144.

(54) Filleter, T.; Mcchesney, J. L.; Bostwick, A.; Rotenberg, E.; Emtsev, K. V.; Seyller, T.; Horn, K.; Bennewitz, R. Friction and Dissipation in Epitaxial Graphene Films. *Phys. Rev. Lett.* **2009,** *102* (8), 086102-086106.

(55) Jr, E. M. K. Damping of Flexural Waves by a Constrained Viscoelastic Layer. *Acoustical*

Society of America Journal **2005,** *31* (7), 952-962.

(56) Yang, X. Y.; Wang, X. B.; Jing, L. I.; Yang, J.; Wan, L.; Wang, J. C. Controllable Reduction and Structural Characterizations of Graphene Oxides. *Chemical Journal of Chinese Universities* **2012,** *33* (9), 1902-1907.

(57) He, H.; Klinowski, J.; Forster, M.; Lerf, A. A New Structural Model for Graphite Oxide. *Chem. Phys. Lett.* **1998,** *287* (12), 53-56.

(58) Eigler, S.; Feicht, P. Defects in Graphene Oxide as Structural Motive. *Chemnanomat* **2017,** *4*, 1-10.

(59) Zandiatashbar, A.; Lee, G. H.; An, S. J.; Lee, S.; Mathew, N.; Terrones, M.; Hayashi, T.; Picu, C. R.; Hone, J.; Koratkar, N. Effect of Defects on the Intrinsic Strength and Stiffness of Graphene. *Nature Communications* **2014,** *5*, 3186-3195.

(60) Mao, Y.; Wen, S.; Chen, Y.; Zhang, F.; Panine, P.; Chan, T. W.; Zhang, L.; Liang, Y.; Liu, L. High Performance Graphene Oxide Based Rubber Composites. *Sci. Rep.* **2013,** *3* (3), 2508-2515.

(61) Vilaverde, C.; Santos, R. M.; Paiva, M. C.; Covas, J. A. Dispersion and Re-Agglomeration of Graphite Nanoplates in Polypropylene Melts under Controlled Flow Conditions. *Composites Part A* **2015,** *78*, 143-151.

(62) Yu, B.; Shi, Y.; Yuan, B.; Liu, L.; Yang, H.; Tai, Q.; Lo, S.; Song, L.; Hu, Y. Click-Chemistry Approach for Graphene Modification: Effective Reinforcement of UV-Curable Functionalized Graphene/Polyurethane Acrylate Nanocomposites. *Rsc Advances* **2015,** *5* (18), 13502-13506.

(63) Shamsi, R.; Koosha, M.; Mahyari, M. Improving the Mechanical, Thermal and Electrical Properties of Polyurethane - Graphene Oxide Nanocomposites Synthesized by In-situ Polymerization of Ester-Based Polyol with Hexamethylene Diisocyanate. *Journal of Polymer Research* **2016,** *23* (12), 262-273.

(64) Abbasi, A.; Sadeghi, G. M. M.; Ghasemi, I.; Shahrousvand, M. Shape Memory Performance of Green In-situ Polymerized Nanocomposites Based on Polyurethane/Graphene Nanoplatelets: Synthesis, Properties, and Cell Behavior. *Polym. Compos.* **2017,** *10*, 4020-4033.

(65) Han, S.; Chun, B. C. Preparation of Polyurethane Nanocomposites via Covalent Incorporation of Functionalized Graphene and Its Shape Memory Effect. *Composites Part A* **2014,** *58* (58), 65-72.

(66) Hummer, W. S.; Offeman, R. E. Functionalized Graphene and Graphene Oxide: Materials Synthesis and Electronic Applications. *J. Am. Chem. Soc.* **1958,** *80*.